

# Experimental Demonstrations of Coherence de Broglie Wavelength for Scalable Superresolution with Near-perfect Fringe Visibility

Sangbae Kim<sup>1,2</sup> and Byoung S. Ham<sup>1,3,\*</sup>

<sup>1</sup>Department of Electrical Engineering and Computer Science, Gwangju Institute of Science and Technology, 123 Chumdangwagi-ro, Buk-gu, Gwangju 61005, S. Korea

<sup>2</sup>QSIM+, 145 Anam-ro, Sungbuk-gu, Seoul 02841, S. Korea

<sup>3</sup>Department of Electrical and Computer Engineering, Oregon State University, Corvallis, OR 97331, USA  
(Submitted on March 12, 2026; \*bham@gist.ac.kr)

**Abstract:** Quantum sensing and metrology have been intensively studied over the last several decades to surpass the fundamental shot-noise limit of classical systems and approach the Heisenberg limit. However, implementation of N00N-state-based quantum sensing has been severely constrained by the limited order  $N$ , intrinsically imperfect fringe visibility, and vulnerability to photon loss. Recently, the coherence de Broglie wavelength (CBW) has been proposed as an alternative method for achieving superresolution in a coherently coupled interferometer architecture, whose characteristics resemble those of photonic de Broglie wavelength (PBW) used in quantum sensing. Here, we experimentally demonstrate scalable CBW superresolution up to  $N = 3$ , with near-perfect fringe visibility that is invariant to photon loss. The observed CBWs have the potential to enable a superresolution sensing platform even if it remains within the shot-noise limit.

## Introduction

Precision measurements have been a last long research topic in a wide range of scientific and technological areas, including spectroscopy, imaging, sensing, and metrology. The performance of classical optical systems is fundamentally limited by the diffraction limit in resolution and statistical noise in sensitivity [1-3]. The diffraction limit constrains spatial and phase resolution to approximately half the wavelength of the probing light, while measurement sensitivity is bounded by the shot-noise limit (SNL) [4] arising from photon-number fluctuations [5]. Overcoming these classical limits has been a major motivation for the development of quantum sensing and quantum metrology. Quantum metrology exploits nonclassical properties of light such as entanglement and squeezing to enhance measurement performance [5-9]. In particular, maximally path-entangled N00N states produce interference fringes with an effective wavelength  $\lambda/N$ , known as the photonic de Broglie wavelength (PBW), enabling ideally superresolution and, in principle, supersensitivity given by the Heisenberg limit in sensitivity scaling [10-12]. Despite these theoretical advantages, PBW-based approaches face significant practical limitations. High-order entangled photon states are difficult to generate and maintain, and their interference visibility rapidly deteriorates in the presence of photon loss and decoherence. As a result, the scalability of PBW-based quantum sensing remains severely restricted [13-15].

An alternative route to superresolution has recently been proposed in the name of the coherence de Broglie wavelength (CBW) [16,17]. In contrast to PBW, CBW arises from deterministic higher-order coherence rather than multiphoton entanglement. This coherence-based mechanism produces an effective wavelength scaling analogous to PBW while avoiding the need for fragile entangled states. Because CBW relies on classical coherence properties of optical fields, it is intrinsically more robust against photon loss and experimental imperfections. While CBW does not achieve supersensitivity beyond the standard quantum limit, analytical studies have shown that it can still provide enhanced phase sensitivity relative to conventional interferometric measurements while maintaining superresolution [18]. Importantly, CBW predicts several key advantages over PBW, including scalable order dependence, near-unity fringe visibility independent of interference order, and strong invariance to photon loss. These features suggest that CBW may provide a practical pathway toward scalable superresolution sensing and metrology without the severe resource requirements associated with quantum-entangled states. A recent quantum mechanical analysis further clarified the physical origin of CBW and its relationship to higher-order interference phenomena in quantum optics.

Here we report an experimental demonstration of CBWs up to order  $N=3$  in both the single-photon and continuous-wave regimes. The observed interference patterns exhibit the predicted wavelength reduction proportional to  $1/N$  while maintaining near-perfect visibility across different interference orders. Furthermore, the

measured signals show strong robustness against photon loss, confirming a key advantage of CBW over PBW-based implementations. These results provide direct experimental validation of the CBW framework and establish coherence-based interferometry as a promising platform for practical superresolution sensing.

## Results

### Theory

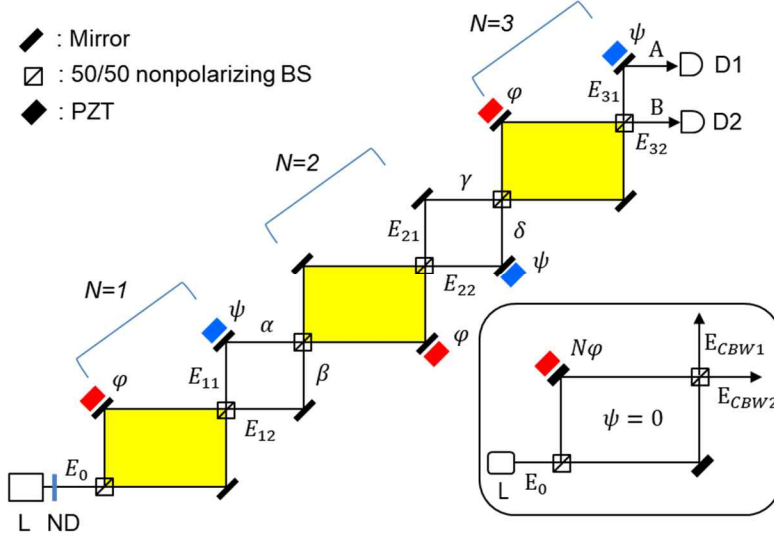


**Fig. 1. Schematic of Nth-order CBW.** L: Laser, ND: neutral density filters, D: single-photon detector, CCU: coincidence counting module. The input field  $E_0$  is an attenuated continuous-wave laser at 100  $\mu$ W. For CBW, the  $\psi = 0$ . Inset: Effective MZI for CBW sensing.

Figure 1 shows a schematic of the scalable CBW scheme implemented in a triply coupled Mach-Zehnder interferometer (MZI) architecture to experimentally achieve PBW-like superresolution in the classical regime. The role of asymmetric coupling between adjacent MZIs indexed by  $N = 1, 2, 3$  in the cascaded MZI structure is to match the same path basis of the MZIs, resulting in the  $N$ th power of the MZI unitary operator [18]. For this purpose, the dummy MZI ( $\psi$ ) is essential to satisfy  $D^\dagger \sigma_z D = \sigma_z$ , where  $\sigma_z$  is the Pauli operator and  $D$  denotes the dummy MZI satisfying  $[D, \sigma_z] = 0$ . Here, the asymmetric coupling represents a  $\pi$ -phase shift between adjacent  $\varphi$ -MZIs [16]. The same asymmetry can also be achieved by controlling  $\psi$  of the dummy MZIs for the identical  $\varphi$ -MZIs (see Section A of the Supplementary Materials).

The physics of CBW refers to the wave nature of a single photon in quantum mechanics; thus, CBW is intrinsically compatible with coherence optics. In contrast, the physics of PBW utilizes the particle nature of photons, where the corresponding superresolution is generated by photon-to-photon correlations of  $N00N$  states acting within the same single MZI. Although CBW differs fundamentally from PBW in its physical mechanism, these features can be understood in terms of the wave-particle duality in quantum mechanics. Unlike PBW-based quantum sensing, CBW superresolution is not affected by the photon loss in measurements. In addition, CBW exhibits near-perfect fringe visibility regardless of the order  $N$ . These features make CBW effective for implementing superresolution sensing with  $N$ -enhanced sensitivity, even though CBW remains within SNL [18].

The input field  $E_0$  in Fig. 1 is provided by a commercially available laser (L). Neutral density filters (ND) are used to control the intensity of  $E_0$  (see Methods). For the experimental demonstrations of CBW superresolution, we first demonstrate scalable CBWs in a single-photon regime up to  $N = 3$  (see Section B of the Supplementary Materials). Unlike PBWs, in which entangled photon pairs occupy both input ports of the first MZI, CBW uses only one input port, while the other port is open to vacuum noise. As analyzed quantum mechanically, CBW superresolution does not surpass SNL in the scaling of the random variable [18]. Secondly,

we experimentally repeat the CBW superresolution using continuous-wave (CW) light, and the results are compared with those obtained from single-photon-based CBWs. Finally, analytic solutions and numerical calculations are performed to support the observed CBWs.

For the measurement of CBW superresolution in the single-photon regime, the coincidence-detection technique used in quantum sensing is adopted to isolate single photons from Poisson-distributed photon events (see Section B of the Supplementary Materials). As in N00N-state-based quantum sensing, the independent and identically distributed (*i.i.d.*) photons in measurements are ensured by a 50/50 nonpolarizing beam splitter (BS), whose output ports are randomly populated. Multiple photons arriving within the same detection time window of a single-photon detector may induce probabilistic errors unless photon-number-resolving detectors are used. Since the origin of this statistical error lies in the Poisson-distribution of photons, the intrinsic error in single-photon detection is typically only a few percent. Nevertheless, this statistical measurement error does not affect the observed CBW fringe visibility, because the MZI unitary transformation depends only on the relative phase  $\varphi$ , not on the input photon number or detected photon number. This property highlights the essence of coherence-optics-based CBW sensing and metrology.

To demonstrate the first-order ( $N = 1$ ) CBW superresolution in Fig. 1, the output fields  $E_{11}$  and  $E_{12}$  are measured to obtain the first-order intensity correlation, resulting in CBW fringes. These fringes arise from the unitary transformation of a single photon or the input field  $E_0$ , which is quantum mechanically represented by  $e^{i\pi\sigma_x/2}$ , where  $\sigma_x$  is the Pauli operator [18]. It is well known that an MZI behaves like a qubit system, where the Pauli matrices generate the unitary operations acting on the path basis:

$$U_{MZI}(\varphi) = BP(\varphi)B = e^{i\varphi/2} \begin{bmatrix} \cos\left(\frac{\varphi}{2}\right) & i\mathbf{\hat{n}} \left(\frac{\varphi}{2}\right) \\ i\mathbf{\hat{n}} \left(\frac{\varphi}{2}\right) & \cos\left(\frac{\varphi}{2}\right) \end{bmatrix}, \quad (1)$$

where  $B = e^{i\pi\sigma_x/4}$  and  $P(\varphi) = e^{i\varphi\sigma_z/2}$ . In Eq. (1), the first-order CBW is expressed as  $\lambda_{CBW}^{(1)} = \lambda_0$ , where  $\lambda_0$  is the wavelength of the input field.

For the second-order ( $N = 2$ ) CBW superresolution, expressed as  $\lambda_{CBW}^{(2)} = \lambda_0/2$ , the output fields  $E_{21}$  and  $E_{22}$  are measured using the same first-order intensity correlation. However, in this case, the unit MZI transformation is doubled in the cascaded structure, resulting in a phase-doubling effect [18]:

$$U_{MZI}^{(2)}(\varphi) = (U_{MZI}(\varphi))^{\otimes 2} = e^{i\varphi} \begin{bmatrix} \cos\varphi & i\mathbf{\hat{n}}\varphi \\ i\mathbf{\hat{n}}\varphi & \cos\varphi \end{bmatrix}. \quad (2)$$

In Eq. (2), the measured output fringes of  $E_{21}$  and  $E_{22}$  are doubled compared with those of  $E_{11}$  and  $E_{12}$  in Eq. (1).

For the third-order ( $N = 3$ ) CBW superresolution, the output fields  $E_{31}$  and  $E_{32}$  correspond to the tripled MZI unitary transformations, resulting in a tripled phase accumulation:

$$U_{MZI}^{(3)}(\varphi) = (U_{MZI}(\varphi))^{\otimes 3} = e^{i3\varphi/2} \begin{bmatrix} \cos\left(\frac{3\varphi}{2}\right) & i\mathbf{\hat{n}} \left(\frac{3\varphi}{2}\right) \\ i\mathbf{\hat{n}} \left(\frac{3\varphi}{2}\right) & \cos\left(\frac{3\varphi}{2}\right) \end{bmatrix}. \quad (3)$$

Equation (3) shows the  $N = 3$  CBW superresolution, resulting in  $\lambda_{CBW}^{(3)} = \lambda_0/3$ . As analyzed quantum mechanically [18], the intensity of the  $N$ th-order CBW superresolution follows the first-order intensity correlation,  $(1 \pm \alpha s(N\varphi))/2$ , exhibiting order-independent fringe visibility. Unlike PBW, the observed CBWs in Fig. 2 confirm their invariance to photon loss in measurements (not shown). Compared with PBW, these factors offer a significant advantage for a CBW-based superresolution sensing platform.

To understand the uniqueness of CBW superresolution, as analyzed in Eqs. (1)-(3), the normal mode of a coupled classical system - such as a standard spring-mass chain - can be considered for comparison. The exact solution is  $\omega_p = 2\sqrt{\frac{k}{m}} \mathbf{\hat{n}} \left(\frac{p\pi}{2(N+1)}\right)$ , where  $m$  and  $k$  denote the mass and spring constant, respectively, and  $p = 1, 2, \dots, N$ . The resulting classical normal mode  $\omega_p$  is not linear in  $N$ , although it may appear approximately linear for low orders. In fact, no classical counterpart of CBW superresolution has been identified.

## Experiments

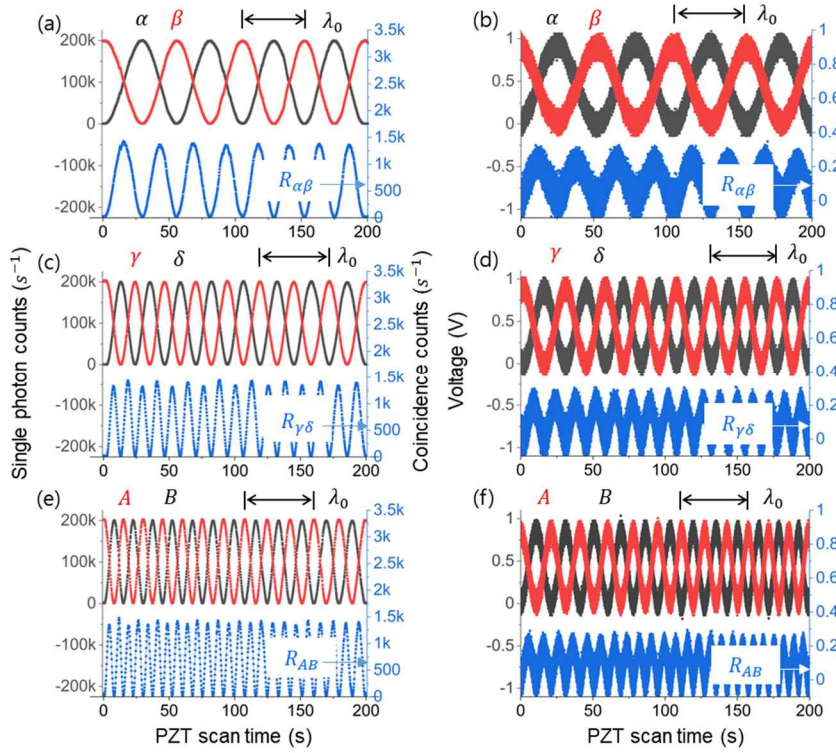


**Fig. 2. Experimental results of CBW in Fig. 1.** (a),(c),(e) single photon cases (see Methods). (b),(d),(f) CW cases at 100  $\mu\text{W}$  cw power of 532 nm laser. The right vertical axis of each panel is for the coincidence count rate for  $R_{ij}$ , where  $i$  and  $j$  are the corresponding output pairs. The horizontal-axes are for the synchronized  $\varphi_s$ , where the phase of  $\varphi_s$  is controlled by PZT via a PZT controller (see Methods). From the top to the bottom rows,  $n=1$ ,  $n=2$ , and  $n=3$ , respectively.

Figure 2 shows the experimental results of the CBW superresolution for  $N = 1, 2, 3$  obtained from the asymmetrically coupled MZI architecture in Fig. 1 under the  $\psi = 0$  condition of the dummy MZI. The left column of Fig. 2 corresponds to the single-photon regime, where different orders of CBWs are measured separately under a common scanning condition of synchronized piezoelectric transducers (PZTs), which is equivalent to the phase  $\varphi$  in Eqs. (1)-(3) (see Methods). The right column of Fig. 2 corresponds to the CW cases with an input power of 0.1 mW for  $E_0$ , using the same PZT scanning condition as the single-photon case. As observed, both  $N$ -dependent fringes satisfy the superresolution relation  $(1 \pm \alpha s (N\varphi))/2$  with near-perfect fringe visibility (see details in Table 1). The fringe period  $\lambda_0$  in the top row of both cases represents the wavelength of the input field  $E_0$  as a reference (see Figs. 2(a) and 2(b)). The coincidence measurement  $R_{\alpha\beta}$  in the left column is directly read out from the coincidence counting unit (CCU; Altera DE2) for the second-order intensity correlation of the output signals  $\alpha$  and  $\beta$ , detected by corresponding single-photon counting modules (Excelitas AQRH-SPCM-15). The corresponding  $R_{\alpha\beta}$  in Fig. 2(b) for the CW case is obtained by calculating the product of the individual CW-output fields  $\alpha$  and  $\beta$ . This calculation was performed in Excel due to the lack of dedicated hardware.

Figures 2(c) and 2(d) show the experimental results of the second-order ( $N = 2$ ) CBW superresolution, where the fringe period is shortened to one half of that in Figs. 2(a) and 2(b). Thus, the CBW superresolution for  $N = 2$  can be represented as  $\lambda_{CBW}^{(2)} = \lambda_0/2$ , with the fringe visibility remaining near perfect, as observed (see Table 1). Likewise, Figs. 2(e) and 2(f) present the experimental results of the third-order ( $N = 3$ ) CBW superresolution, satisfying  $\lambda_{CBW}^{(3)} = \lambda_0/3$ . Similarly, both the single-photon and CW CBWs exhibit near-perfect fringe visibility (see Table 1). Due to the wave nature of CBW, the photon-loss vulnerability this is critical in

PBW-based quantum sensing is no longer relevant (not shown). Moreover, Fig. 2 demonstrates that a particular order of CBW is automatically selected by setting the number of  $\varphi$ -MZIs, owing to the asymmetrically coupled-MZI physics with SU(2) symmetry [18]. In contrast, N00N-state-based PBWs are inherently difficult to isolate from hyper-Poisson-distributed N00N states, resulting in inevitably imperfect fringe visibility [14,15]. Finally, the observed CBW superresolution in Fig. 2 demonstrates the quantized phase basis of CBW at  $\varphi_N = m\pi/N$ , where  $m=0,1,2,\dots,N$  (discussed below) [2]. This CBW phase quantization is mathematically equivalent to the Pegg-Barnett formalism of the phase operator [19].

**Table 1. Measured CBW visibilities for Fig. 2.** The i (j) stands for  $\alpha$  ( $\beta$ ),  $\gamma$  ( $\delta$ ), and A (B) in each order in Fig. 2.

Case \ Order		$N = 1$	$N = 2$	$N = 3$
Single photon	Red	$98.36 \pm 0.12$	$99.51 \pm 0.07$	$98.47 \pm 0.14$
	Blue	$99.40 \pm 0.12$	$99.56 \pm 0.01$	$99.25 \pm 0.04$
CW	Red	$100 \pm 0.0$	$98.14 \pm 0.95$	$100 \pm 0.0$
	Blue	$98.88 \pm 0.52$	$100 \pm 0.0$	$97.40 \pm 0.83$

#### Coherence solution of CBW

From Fig. 1, the following analytical solutions are derived from MZI matrix representations:

$$\begin{bmatrix} E_A \\ E_B \end{bmatrix} = [\varphi^+][M^+] \begin{bmatrix} E_\gamma \\ E_\delta \end{bmatrix}, \quad (4)$$

where  $\begin{bmatrix} E_\gamma \\ E_\delta \end{bmatrix} = [\varphi^-][M^-] \begin{bmatrix} E_\alpha \\ E_\beta \end{bmatrix}$ ,  $\begin{bmatrix} E_\alpha \\ E_\beta \end{bmatrix} = [\varphi^+][M^+] \begin{bmatrix} E_0 \\ 1 \end{bmatrix}$ ,  $[M^+] = \frac{1}{2} \begin{bmatrix} (1 - e^{i\psi}) & i(1 + e^{i\psi}) \\ i(1 + e^{i\psi}) & -(1 - e^{i\psi}) \end{bmatrix}$ ,  $[M^-] = \frac{1}{2} \begin{bmatrix} -(1 - e^{i\psi}) & i(1 + e^{i\psi}) \\ i(1 + e^{i\psi}) & (1 - e^{i\psi}) \end{bmatrix}$ ,  $[\varphi^+] = \begin{bmatrix} 1 & 0 \\ 0 & e^{i\psi} \end{bmatrix}$ , and  $[\varphi^-] = \begin{bmatrix} e^{i\psi} & 0 \\ 0 & 1 \end{bmatrix}$ . For the coherence optics-based analytic solutions,  $\psi = 0$  is set for all dummy MZIs.

From Eq. (4), the following CBW relations can be derived:

$$\begin{bmatrix} E_\alpha \\ E_\beta \end{bmatrix} = \frac{1}{2} \begin{bmatrix} (1 - e^{i\psi}) & i(1 + e^{i\psi}) \\ i(1 + e^{i\psi}) & -(1 - e^{i\psi}) \end{bmatrix} \begin{bmatrix} E_0 \\ 0 \end{bmatrix}, \quad (5)$$

$$\begin{bmatrix} E_\gamma \\ E_\delta \end{bmatrix} = \frac{1}{4} \begin{bmatrix} -(1 - e^{i\psi}) & i(1 + e^{i\psi}) \\ i(1 + e^{i\psi}) & (1 - e^{i\psi}) \end{bmatrix} \begin{bmatrix} (1 - e^{i\psi}) & i(1 + e^{i\psi}) \\ i(1 + e^{i\psi}) & -(1 - e^{i\psi}) \end{bmatrix} \begin{bmatrix} E_0 \\ 0 \end{bmatrix}, \quad (6)$$

$$\begin{bmatrix} E_A \\ E_B \end{bmatrix} = \frac{1}{8} \begin{bmatrix} (1 - e^{i\psi}) & i(1 + e^{i\psi}) \\ i(1 + e^{i\psi}) & -(1 - e^{i\psi}) \end{bmatrix} \begin{bmatrix} -(1 - e^{i\psi}) & i(1 + e^{i\psi}) \\ i(1 + e^{i\psi}) & (1 - e^{i\psi}) \end{bmatrix} \begin{bmatrix} (1 - e^{i\psi}) & i(1 + e^{i\psi}) \\ i(1 + e^{i\psi}) & -(1 - e^{i\psi}) \end{bmatrix} \begin{bmatrix} E_0 \\ 0 \end{bmatrix}. \quad (7)$$

Equation (5) yields  $I_\alpha = I_0(1 - \cos\psi)/2$  and  $I_\beta = I_0(1 + \cos\psi)/2$ , where  $I_j = E_j E_j^*$ . These correspond to the typical MZI interference fringes, equivalent to the first-order CBW superresolution. Likewise, Eq. (6) yields  $I_\gamma = I_0(1 + \cos(2\psi))/2$  and  $I_\delta = I_0(1 - \cos(2\psi))/2$ , indicating the second-order CBW superresolution. Similarly,  $I_A = I_0(1 - \cos(3\psi))/2$  and  $I_B = I_0(1 + \cos(3\psi))/2$  are obtained from Eq. (7) for the third-order CBW superresolution. Thus, the general solution of the Nth-order CBW superresolution can be expressed as:

$$\begin{bmatrix} E_A \\ E_B \end{bmatrix}^{(N)} = (-1)^N \left(\frac{1}{2}\right) \begin{bmatrix} 1 + (-1)^N e^{iN\psi} & -i(1 + (-1)^{N+1} e^{iN\psi}) \\ i(1 + (-1)^{N+1} e^{iN\psi}) & 1 + (-1)^N e^{iN\psi} \end{bmatrix} \begin{bmatrix} E_0 \\ 0 \end{bmatrix}. \quad (8)$$

The corresponding fringes of the Nth-order CBW superresolution can be directly obtained from Eq. (8):

$$I_A^{(N)} = \frac{1}{2}[1 + (-1)^N \cos(N\varphi)], \quad (9)$$

$$I_B^{(N)} = \frac{1}{2}[1 - (-1)^N \cos(N\varphi)]. \quad (10)$$

Equations (9) and (10) agree with the observed data in Fig. 2, satisfying the effective wavelength relation  $\lambda_{A;B} = \frac{\lambda_0}{N}$ . As a result, the Nth-order coincidence measurement becomes  $R_{AB}^{(N)} = I_A^{(N)} \cdot I_B^{(N)} = \frac{1}{4} \sin^2(N\varphi)$ , resulting in doubled fringes (see Fig. 3).

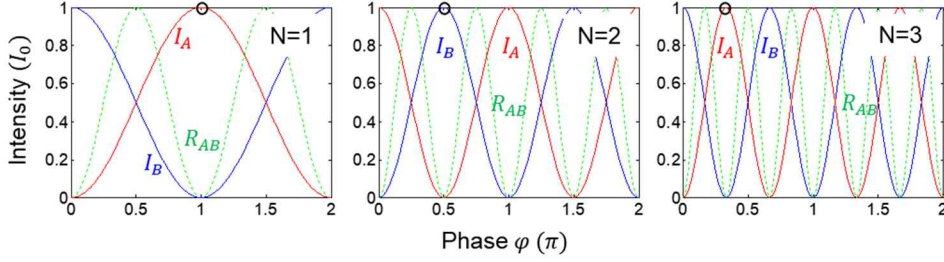


**Fig. 3. Numerical calculations of CBWs for Fig. 2.** The  $N$  represents the number of the basic building block defined in Fig. 1. The open circle indicates the phase basis quantization of the  $N$ -dependent CBWs. The intensity product  $R_{AB}$  is normalized.

Figure 3 shows the corresponding numerical calculations of CBWs at  $\lambda_{CBW} = \frac{\lambda_0}{N}$ , obtained using Eq. (8), to support the experimental data in Fig. 2. The  $(-1)^N$  factor in Eq. (8) appears in the ordered CBWs with a new phase basis  $\varphi_N = m\pi/N$ , where the phase-basis step is  $\Delta\varphi_N = \pi/N$ , as marked by open circles. This leads to an  $N$ -fold increase in resolution according to the Rayleigh criterion. The factor  $(-1)^N$  in Eq. (8) can be interpreted as the eigenvalue of the parity operator  $\hat{P} = (-1)^N$  (discussed elsewhere) [20,21]. Its eigenvalues,  $\pm 1$ , correspond to two quantized phase states  $0$  and  $\pi/N$ , forming a phase basis of the  $N$ -dependent CBW [2]. The open circles in Fig. 3 indicate these phase-basis eigenstates, whose parity-dependent sign determines the constructive output port and results in the  $N$ -fold increase in phase resolution observed in Fig. 2. The intensity product  $R_{AB}^{(N)}$  confirms the analytic solution  $\sin^2(N\varphi)$ , resulting in twice the resolution given by  $\lambda_{CBW}$  (see the green dotted curves). Although CBW has the to enable a new superresolution sensing platform with near-perfect visibility and photon-loss invariance, the phase sensitivity still remains within the SNL of classical physics [18]. Thus, the novelty of the observed CBW superresolution lies in two aspects: first, its compatibility with classical sensing platforms due to its wave nature; and second, its practical advantages over N00N-state-based quantum sensing, which suffers from limited-order scalability [14,15], practically inseparable order  $N$  [15], and photon-loss vulnerability [5-15].

## Conclusion

In conclusion, we experimentally demonstrated scalable ( $N = 1,2,3$ ) CBW superresolution in a triply coupled asymmetric MZI-chain system, where the observed superresolution resembles PBWs in quantum sensing. Unlike PBWs, whose superresolution arises from photon correlations within a single MZI and suffers from imperfect fringe visibility and photon-loss vulnerability, the observed CBW superresolution exhibits order-independent, near-perfect fringe visibility due to the wave nature of quantum mechanics. Most importantly, the scalable CBW superresolution is inherently invariant to the photon loss owing to its coherence-based mechanism. The coherent observation of CBW superresolution in both the single-photon and CW regimes has not been previously reported. Thus, the observed CBW superresolution is fundamentally different from both classical and conventional quantum sensing platforms. For the single-photon-based CBW experiment, a commercially available 532 nm CW laser was optically attenuated to achieve a mean photon number of  $\langle n \rangle \sim 0.04$ , where the single-photon regime was verified

using the coincidence-detection technique commonly employed in quantum sensing. Even with CW laser light, the same near-perfect fringe visibility was experimentally observed, confirming the CBW physics governed by the  $N$ -powered MZI unitary transformation. Analytical solutions were also derived to discuss CBW superresolution using a parity operator, leading to the CBW phase quantization. Under the wave nature of a single photon, the order-dependent phase quantization of CBW is analogous to the energy quantization associated with the particle nature of a single photon. Owing to its determinacy and scalability with order  $N$ , CBW has the potential to overcome the practical limitations of  $N00N$ -state-based quantum sensing and may enable CBW-based superresolution sensing platforms beyond  $N > 100$ . Such platforms could outperform classical counterparts, such as wavemeters and remote sensing systems, even in a photon-loss regimes relevant to modern LiDAR technologies [22,23].

## Methods

For the single photon-based CBW experiments, the input field  $E_0$  was obtained by optically attenuating a 532 nm laser (Coherent, V-10) with an initial power of 100  $\mu\text{W}$  using neutral density filters with an optical density (OD) of 13. As a result, the measured mean photon number was  $\langle n \rangle \sim 0.04$  with respect to the dead time of the single photon detector (Excelitas AQRH-SPCM-15). This mean-photon number was confirmed using both a coincidence counting unit (CCU, Altera DE2) and a fast digital oscilloscope (Yokogawa DL9040; 500 MHz) via a pair of the single photon detectors (see Section B of the Supplementary Materials). For the single-photon CBW experiment, we therefore adopted a coincidence-detection method to suppress the majority of vacuum events. According to photon statistics, however, multiply bunched photons cannot be completely eliminated by this technique, resulting in a statistical error at a few percent in the single photon detection scheme. For the CW CBW experiment, a typical measurement method used in coherence optics was adopted, replacing the coincidence-detection module with avalanche photodiodes (Thorlabs APD 110A). For the PZT scan time of 200 s in Fig. 2, a total of 2.5 million data points were collected from the CCU. Because the PZT was scanned continuously, each data point represents an averaged accumulated over approximately 80  $\mu\text{s}$  of the PZT scan time.

## Acknowledgment

BSH gratefully acknowledges Prof. Ben Lee for hosting the author during the sabbatical leave and for kindly providing office space in the department.

## Data availability

All data generated or analyzed during this study are included in the published article.

## Reference

1. Hell, S. W. Nanoscopy with focused light (Nobel lecture). *Angew. Chem. Int. Ed.* **54**, 8054-8066 (2015).
2. Fujimoto, J. G., Pitris, C., Boppart, S. A. and Brezinski, M. E. Optical coherence tomography: an emerging technology for biomedical imaging and optical biopsy. *Neoplasia* **2**, 9-25 (2000).
3. Hariharan, P. *Optical interferometry*. 2nd Ed. (Academic Press, New York, 2003).
4. Kay, S. *Fundamentals of statistical signal processing: Estimation theory* (Prentice Hall, New Jersey 1993).
5. Degen, C. L., Reinhard, F. & Cappellaro, P. Quantum sensing. *Rev. Mod. Phys.* **89**, 035002 (2017).
6. Pezze, L. *et al.*, Quantum metrology with nonclassical states of atomic ensemble. *Rev. Mod. Phys.* **90**, 035005 (2018).
7. Tse, M. *et al.* Quantum-enhanced advanced LIGO detectors in the era of gravitational-wave astronomy. *Phys. Rev. Lett.* **123**, 231107 (2019).
8. Dowling, J.P. Quantum optical metrology—The lowdown on high- $N00N$  states. *Contemp. Phys.* **49**, 125–143 (2008).
9. Giovannetti, V., Lloyd, S. & Maccone, L. Quantum-enhanced measurements: beating the standard quantum limit. *Science* **306**, 1330-1336 (2004).
10. Jacobson, J., Gjørk, G., Chung, I. & Yamamoto, Y. Photonic de Broglie waves. *Phys. Rev. Lett.* **74**, 4835-4838 (1995).

11. Walther, P., Pan, J.-W., Aspelmeyer, M., Ursin, R., Gasparon, S. & Zeilinger, A. De Broglie wavelength of a non-local four-photon state. *Nature* **429**, 158-161 (2004).
12. Leibfried, D. et al. Toward Heisenberg-limited spectroscopy with multiparticle entangled states. *Science* **304**, 1476-1478 (2004)
13. Wang, X.-L. et al., 18-qubit entanglement with six photons' three degree of freedom. *Phys. Rev. Lett.* **120**, 260502 (2018).
14. Nagata, T., Okamoto, R., O'Brian, J. L., Sasaki, K. & Takeuchi, S. "Beating the standard quantum limit with four-entangled photons," *Science* **316**, 726–729 (2007).
15. Sun, F. W. et al. Experimental demonstration of phase measurement precision beating standard quantum limit by projection measurement. *EPL* **82**, 24001 (2008).
16. Ham, B. S. Deterministic control of photonic de Broglie waves using coherence optics. *Sci. Rep.* **10**, 12899 (2020).
17. Ham, B. S. Analysis of nonclassical features in a coupled macroscopic binary system. *New J. Phys.* **22**, 123043 (2020).
18. Ham, B. S. A quantum mechanical analysis of the coherence de Broglie wavelength for superresolution and enhanced sensitivity in a coupled interferometer scheme *arXiv:2602.20410* (2026).
19. Pegg, D. T. & Barnett, S. M. Phase properties of the quantized single mode electromagnetic field. *Phys. Rev. A* **39**, 1665-1675 (1989).
20. Gerry, C. C. & Mimih, J. The parity operator in quantum optical metrology. *Contemporary Physics* **51**, 497–511 (2010).
21. Anisimov, P. et al. Quantum metrology with two-mode squeezed vacuum: parity detection beats the Heisenberg limit. *Phys. Rev. Lett.* **104**, 103602 (2010).
22. Charbon, E., Fissburn, M., Walker, R., Henderson, R. K. & Niclass, C. *SPAD-based sensors*, Eds. F. Remondino and D. Stoppa (Springer-Verlag, Berlin, 2013).
23. Scholes, S., Mora-Martin, G., Zhu, F., Gyongy, I., Soan, P. & Leach, J. Fundamental limits to depth imaging with single-photon detector array sensors," *Sci. Rep.* **13**, 176 (2023).

### **Funding**

BSH acknowledges that this work was supported by the IITP-ITRC grant (IITP 2026-RS-2021-II211810) funded by the Korean government (Ministry of Science and ICT).

### **Author contribution**

B.S.H. conceived the idea, analyzed the data with numerical calculations, and wrote the manuscript. S.K. conducted the experiments and analyzed the related data. Correspondence and request of materials should be addressed to BSH (email: bham@gist.ac.kr).

### **Competing interests**

BSH is the founder of Qu-Lidar.

**Supplementary information** is available in the online version of the paper.